Single Crystalline La$_{0.7}$Sr$_{0.3}$MnO$_3$ Molecular Sieve Nanowires with High Temperature Ferromagnetism

Adrián Carretero-Genevrier,[†] Jaume Gázquez,[‡,§] Juan Carlos Idrobo,[‡,||] Judith Oró,[†] Jordi Arbiol,[†,⊥] María Varela,[‡] Etienne Ferain,[#] Juan Rodríguez-Carvajal,[&] Teresa Puig,[†] Narcís Mestres,*,[†] and Xavier Obradors[†]

[†]Institut de Ciència de Materials de Barcelona ICMAB, Consejo Superior de Investigaciones Científicas CSIC, 08193 Bellaterra, Catalonia, Spain

[‡]Materials Science and Technology Division, Oak Ridge National Laboratory, Oak Ridge, Tennessee 37831, United States

[§]Departamento de Física Aplicada III, Universidad Complutense de Madrid, Madrid, 28040, Spain

[||]Department of Physics and Astronomy, Vanderbilt University, Nashville, Tennessee 37235, United States

[⊥]Institució Catalana de Recerca i Estudis Avançats (ICREA)

[#]Institute of Condensed Matter and Nanosciences, Bio & Soft Matter (IMCN/BSMA), Université catholique de Louvain, Croix du Sud 1,1348 Louvain-la-Neuve, Belgium, and it4ip s.a., rue J. Bordet (Z.I. C), 7180 Seneffe, Belgium

[&]Institut Laue-Langevin, 6 rue Jules Horowitz, BP 156, 38042 Grenoble Cedex 9, France

S *Supporting Information*

ABSTRACT: Porous mixed-valent manganese oxides are a group of multifunctional materials that can be used as molecular sieves, catalysts, battery materials, and gas sensors. However, material properties and thus activity can vary significantly with different synthesis methods or process conditions, such as temperature and time. Here, we report on a new synthesis route for MnO$_2$ and LaSr-doped molecular sieve single crystalline nanowires based on a solution chemistry methodology combined with the use of nanoporous polymer templates supported on top of single crystalline substrates. Because of the confined nucleation in high aspect ratio nanopores and of the high temperatures attained, new structures with novel physical properties have been produced. During the calcination process, the nucleation and crystallization of ε-MnO$_2$ nanoparticles with a new hexagonal structure is promoted. These nanoparticles generated up to 30 μm long and flexible hexagonal nanowires at mild growth temperatures (T_g = 700 °C) as a consequence of the large crystallographic anisotropy of ε-MnO$_2$. The nanocrystallites of MnO$_2$ formed at low temperatures serve as seeds for the growth of La$_{0.7}$Sr$_{0.3}$MnO$_3$ nanowires at growth temperatures above 800 °C, through the diffusion of La and Sr into the empty 1D-channels of ε-MnO$_2$. Our particular growth method has allowed the synthesis of single crystalline molecular sieve (LaSr-2 × 4) monoclinic nanowires with composition La$_{0.7}$Sr$_{0.3}$MnO$_3$ and with ordered arrangement of La^{3+} and Sr^{2+} cations inside the 1D-channels. These nanowires exhibit ferromagnetic ordering with strongly enhanced Curie temperature (T_c > 500 K) that probably results from the new crystallographic order and from the mixed valence of manganese.
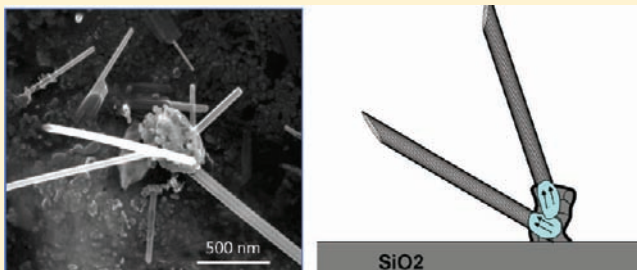
■ INTRODUCTION

Magnetic materials are well-known for a number of interesting applications in both low and high technology sectors, including information storage and sensor applications. Nowadays, several magnetic technologies have emerged relying on the control at the nanoscale of spin polarization and its manipulation by electric and magnetic fields or light.[1,2] More specifically, the study of the transport properties of manganese oxides has proved to be a fruitful area of research in recent years where the nanoscale properties have not yet been exploited and understood fully.[3,4] Of particular importance has been the observation of colossal magnetoresistance in a number of mixed valence La$_{1-x}$A$_x$MnO$_3$ (A = Ca, Ba, or Sr)

oxides with the perovskite[4] and pyrochlore[5] structures. For practical device applications, magnetic materials should exhibit a Curie point (T_c) well above room temperature, which is nowadays a bottleneck issue for many practical applications. A variety of oxides, including mixed-valence perovskite manganites,[3,4] diluted magnetic oxides,[6] spinels,[7] ferrites,[8] and double perovskites,[9] have been studied, but success in rising T_c has been scarce.

In addition to the perovskite manganese oxides, where mixed-valent Mn plays a determinant role in the magnetic and transport

properties, there is another important group of functional materials based on manganese oxides where the Mn ions are in mixed-valence state. These manganese oxides with the general formula A_xMnO_2 have porous structures, open tunnels, and high surface areas. The building blocks are MnO_6 octahedra, and these octahedra share their corners and edges to form channel-like slabs and further cross-link to build 1-D tunnels. The A-cations reside in the pores to support the framework and to maintain charge balance. This family of materials is also known as manganese oxide octahedral molecular sieves (OMS).[10,11] Recently, much effort has been devoted to synthesize novel nanoscale manganese oxide OMS and metal-substituted OMS materials to modify their physical and chemical properties and to improve their performance as electrodes for batteries and super-capacitors, as well as redox catalysts.[12−15] Additionally, the magnetic properties of one-dimensional (1-D) nanostructured Mn oxides have been investigated only in a few of these cases. Some of these Mn oxides are ferromagnetic at low temperature, with Curie temperatures not exceeding 40 K.[16−18]

The controlled synthesis of ternary and quaternary metal oxide nanorods and nanowires is, however, notoriously more problematic due to the difficulty in controlling the precursor reactions and achieving a homogeneous final stoichiometry. As a result, only limited success has been obtained on a few materials,[19,20] and up to now the synthesis of nanowires of multicomponent oxides is still a challenging issue. In this context, chemical solution methods are very appealing because they offer a precise control over stoichiometry and have been proven to be a highly flexible procedure for the fabrication of electronic oxide films and nanostructures.[20−23] Developing approaches to pre-pare single crystalline oxide nanostructures from solution chem-istry has been the recent focus of our efforts.[24−27] The combination of solutions and template-inspired methodologies represents a convenient and versatile method for generating 1D nanostructures. However, most nanostructures produced by conventional hard templating procedures are polycrystalline, despite the variety of different deposition strategies used.[28−30] The reason for the observed polycrystallinity is the heteroge-neous nucleation on the pore walls during the annealing step.

Here, we report on a new synthesis method for single crystal-line MnO_2 and $La_{0.7}Sr_{0.3}MnO_3$ (LSMO) nanowires using a polymer-based precursor solution and the nanopores of track-etched polymer templates as nanoreactors. At mild growth temperatures ($T_g = 700$ °C), up to 30 μm long MnO_2 nanowires are generated. At higher temperatures ($T_g \approx 800−1000$ °C), single crystalline LSMO nanowires are formed. These nanowires show a new monoclinic crystallographic structure related to the structure of synthetic 2 × 4 tunnel manganates,[31,32] with the La and Sr cations arranged within the channels of the manganate framework. This new crystallographic structure is at the origin of the observed high temperature ferromagnetism, with a nano-wire's Curie temperature well above 500 K. The method devel-oped in this work offers an efficient approach for the low-cost and large-scale synthesis of MnO_2 and LSMO nanowires for realistic and practical applications in nanoscience and technology and without the involvement of any catalyst impurity.

■ EXPERIMENTAL METHODS

Sample Preparation. Polycarbonate (PC) films were deposited on silicon substrates by spin coating at 4500 rpm using a 10% w/v PC solution in chloroform. Spin-coated templates were therefore annealed at 190 °C under a vacuum for 4 h to improve PC layer adhesion to the substrates. The supported PC layers were then beamed in the accelerator of the Cyclotron Research Center at Louvain-la-Neuve with energetic heavy ions (Ar^{9+} at 5.0 MeV/amu) at fluences from 1×10^6 to 1×10^9 ions/cm^2; this beaming is carried out at around 1×10^{-2} mbar and at room temperature. Tracks created in polymer layers by energetic heavy ions were revealed into pores by a selective etching with a 0.5 N NaOH aqueous solution at 70 °C for a time depending on the requested final pore size. Before etching, ion irradiated supported layers were UV sensitized to increase etching selectivity and to therefore ensure near cylindrical pore shape. Etching is stopped with an acetic acid solution (15% in water), and porous templates are finally washed into milli-Q water at 70 °C for 5 min minimum before drying with hot air. Pore diameter was designed to be 50 ± 10, 100 ± 10, 200 ± 10, and 300 ± 20 nm with a pore density optimized at 1×10^8 cm^{-2} and a PC porous layer between 1 and 2 μm thick. The supported nanoporous templates were filled by capillary force using a sol−gel-based polymer precursor solution of LSMO, and after the excess of solution was removed by carefully wiping the polymer, the specimens were heated in a furnace at temperatures of 700−1000 °C for 30 min to 5 h in a pure oxygen atmosphere. During this process, the PC polymer (with a decomposition temperature in a single step between 400 and 500 °C) is consequently pyrolyzed.

The LSMO precursor solution was prepared using high purity (>99.99%) metal salts La(NO_3)$_3$·6H_2O, Sr(NO_3)$_2$·4H_2O, and Mn-(NO_3)$_2$·4H_2O. Water used in the solution preparation was purified using the Milli-Q water treatment system. An aqueous solution of nitrates of lanthanum, manganese, and strontium in their stoichiometric ratio was prepared, ethylene glycol was added with continuous stirring, and the whole solution was heated on a hot plate whose temperature was increased gradually to 150 °C. In this way, the polymerized ethylene glycol assists in forming a close network of cations and helps the reaction, enabling the phase formation at low temperatures. The concentration of the final solution was adjusted to 0.9 M in Mn and the viscosity values to η = 30 mPas. The chemical composition of the final solution has been investigated by inductively coupled plasma-atomic emission spectroscopy analysis on a Thermo Elemental Intrepid II XLS (Franklyn, MA) spectrometer.

Sample Characterizations. Field emission electron microscopy (LEO 1530) was used to characterize the morphology and size of the as-synthesized samples. X-ray diffraction measurements were carried out using a Bruker AXS GADDS equipped with a 2D X-ray detector. The microstructure and local chemical composition of the samples was investigated by using a Jeol 1210 transmission electron microscope operating at 120 KV, equipped with a side-entry 60/30° double tilt GATHAN 646 analytical specimen holder and a link QX2000 XEDS element analysis system. STEM-EELS measurements have been ac-quired using a VG Microscopes HB501UX and a NION aberration-corrector, both operated at 100 kV and equipped with an Enfina EEL spectrometer. The specimens for electron microscopy were prepared by dispersion of the nanowires in methanol and deposition of a droplet of this suspension on a holey carbon film supported on a copper grid. High-resolution electron microscopy images were obtained using a Jeol 2011 transmission electron microscope operating at 200 KV and Jeol 2010 FEG transmission electron microscope operating at 200 KV and equipped with a Gatan image filter 200 electron energy-loss spectro-meter with an energy resolution of 0.8 eV.

Magnetization measurements of the nanowires were made in a dc superconducting quantum interference device (SQUID) magnetometer (Quantum Design MPMS-XL7) in fields between 0 and 7 T and from 10 to 400 K, using a sample composed of a Si substrate where the LSMO nanowires were randomly distributed parallel to the substrate. Magne-tization measurements up to 500 K were performed using a vibrating sample magnetometer oven (VSM) model P527. The oven is composed
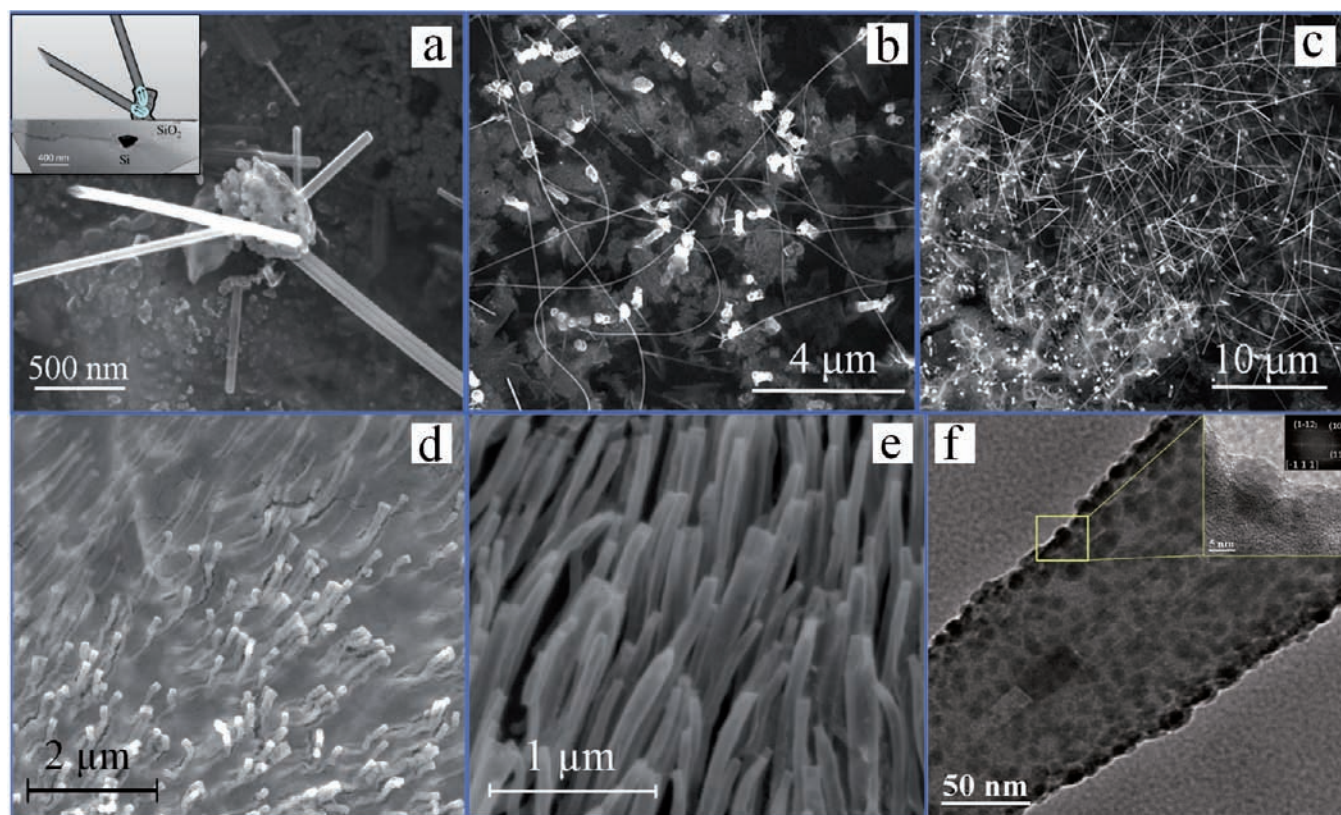
Figure 1. (a) FE-SEM image displaying the growth of nanowires at 700 °C from a vertical nanorod; growth conditions: temperature 700 °C, time 30 min. Inset displays a schematic example of nanowires formation from hexagonal highly anisotropic ε-MnO_2 nanoparticles at 700 °C. The transmission electron microscopy (TEM) cross-sectional image of the interface between the nanorods and the silicon substrate evidences the formation of a thick SiO_2 layer. (b) FE-SEM image shows the formation of nanowires up to 30 μm in length after 2 h of thermal treatment at 700 °C. (c) Large area FE-SEM image of sample (b). FE-SEM images of samples generated at different stages of the thermal treatment: (d) Nanorods formed at 300 °C with diameters of ~100 nm and lengths of ~1.0 μm as determined by the polymer template characteristics. Inset shows a FE-SEM image of a polycarbonate nanoporous membrane deposited on a (001)-silicon substrate with a pore size of 100 nm. (e) Precursor oxides nanorods grown at 500 °C standing on the Si substrate after the template polymer was eliminated by the thermal treatment. (f) High magnification TEM image of an amorphous nanorod of 200 nm grown at 500 °C. The formation of nanoparticles inside the amorphous matrix is observed; inset is the high-resolution TEM image of the ε-MnO_2 nanoparticles formed at 500 °C taken at $[-111]$ zone axis.

of a heater and thermocouple integrated into the vibrating sample rod. During oven operation, a standard VSM detection coilset is used, while the PPMS sample chamber is maintained at 300 K in a high vacuum state ($<10^{-4}$ Torr required). The heated region, including the sample, was wrapped in low emissivity copper foil to minimize heat leak from the hot region to the surrounding coilset.

■ RESULTS AND DISCUSSION

Figure 1 shows field emission scanning electron microscopy (FE-SEM) images of a sample generated from a 1 μm thick polycarbonate (PC) template with pores of diameter 300 nm and a pore density of 1×10^8 cm^{-2} coating a (001)-silicon substrate. After the nanopores were filled with the precursor solution (containing La, Sr, and Mn cations) and a high temperature treatment was performed at 700 °C for 30 min in oxygen atmosphere, the substrate appears covered with vertical nanorods with emerging nanowires in random directions and up to 2 μm in length (see Figure 1a). The inset displays a schematic example of nanowires formation at 700 °C, where a few nanowires emerge from the original nanorod formed inside the nanoporous template at a first stage of thermal treatment. Transmission electron microscopy (TEM) cross-sectional images of interfaces between the nanorods and the silicon

substrates provided evidence that the silicon substrate suffered an oxidation of the surface during the thermal treatment, generating an amorphous SiO_2 layer of ~400 nm. As a consequence, the nanorods stand on top of this amorphous SiO_2 layer. An increase in the growth time led to the formation of very long nanowires up to 30 μm as shown in Figure 1b for a 2 h long growth process. Many of these nanowires are bent due to their high flexibility and aspect ratio. This nanowires formation extends over the whole sample surface as displayed in the larger view of Figure 1c.

To elucidate the formation process of the nanowires, we followed the nucleation and growth steps by studying samples taken at various stages of reaction after thermal treatment at 300 and 500 °C by SEM and TEM measurements. Figure 1d shows a FE-SEM image of the sample grown at 300 °C for 2 h in oxygen atmosphere and generated from 100 nm diameter nanopores. The inset shows a FE-SEM image of a polycarbonate nanoporous membrane deposited on a (001)-silicon substrate with a pore size of 100 nm. We observe the definition of nanorods inside the nanopores of the polymer template. Figure 1e shows a FE-SEM image of a sample generated from a template of the same characteristics as the one in Figure 1d (1 μm thick PC template, pore density 1×10^8 cm^{-2}, and pore diameter 100 nm) after a

4055

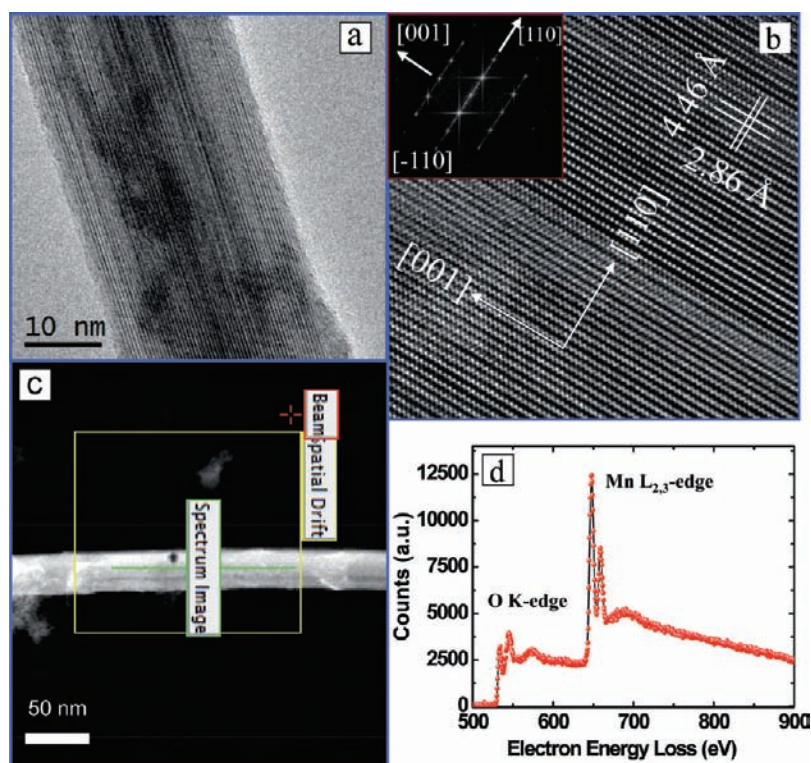dx.doi.org/10.1021/ja1098963 |*J. Am. Chem. Soc.* 2011, 133, 4053–4061

Figure 2. (a) TEM image of a single nanowire grown at 700 °C, 30 min. (b) HRTEM image of a nanowire, where the (001) and (110) interplanar distances are evidenced; the inset shows the FFT pattern, and the zone axis is [−110]. (d) EELS spectrum image generated from the EELS scans across the nanowire displayed in (c), evidencing the MnO_2 composition.

thermal treatment at 500 °C for 2 h in oxygen atmosphere. As a result of the annealing process, the polymer template has been eliminated, and nanorods standing on the Si substrate are formed. The size and density of the nanorods coincide with the original pore size and density in the polymer template. High magnification TEM images of a nanorod generated from a 200 nm nanoporous template (see Figure 1f) show that the nanorods are constituted by an amorphous matrix of La, Sr, Mn, and O, with a considerable amount of nanoparticles having sizes of less than 10 nm. TEM images showed that these nanoparticles display lattice fringes. The selected area electron diffraction (SAED) patterns obtained from single nanoparticles (see inset in Figure 1f) show a lattice spacing close to 2.8 Å.

Further, we have performed the microstructural characterization of the fully formed nanowires at 700 °C by TEM. The measurements revealed that the diameter of the nanowires is between 40 and 50 nm, and that they are structurally uniform and single crystalline (see Figure 2a). Systematic SAED tilting experiments were carried out to investigate the crystalline structure of the nanowires (see Supporting Information Figure 1). The SAED patterns can be indexed on the basis of a hexagonal cell with lattice parameters $a = b = 5.28$ Å, $c = 2.86$ Å, and $\gamma = 120°$. High-resolution TEM (HRTEM) experiments also confirm the single crystalline nature of the nanowires. Figure 2b presents a HRTEM image of a single nanowire along the [−110] zone axis; the inset shows the power spectrum (fast Fourier transform, FFT) of this image in good agreement with the SAED pattern. The interplanar spacing of the nanowires calculated from the FFT is 4.46 Å, corresponding to the (110) crystallographic interplanar distance of the hexagonal unit cell. The shortest interplanar spacing along the nanowires growth direction is 2.86

Å and corresponds to the (001) interplanar distance of the hexagonal unit cell. Electron energy-loss spectroscopy (EELS) analyses (see Figure 2c and d) performed along several nanowires uncover that Mn and oxygen are the only chemical elements present in the nanowires. Moreover, a quantification of the EELS data reveals that in the nanowire the Mn:O ratio is 1:2 over a long lateral length scale (with an error bar of less than 4%, see Supporting Information Figure 3). This confirms that the nanowires grown at 700 °C are hexagonal single crystalline MnO_2 nanowires.

The high magnification TEM measurements performed on the nanoparticles formed at 500 °C evidenced the lattice spacing of 2.86 Å, characteristic of the hexagonal structure demonstrated for MnO_2 nanowires. This observation indicates that hexagonal MnO_2 nanoparticles are formed simultaneously with the decomposition of the PC template in the 360−500 °C temperature interval. Confined nucleation in high aspect ratio nanometric pores might promote a better diffusion of the smaller cation (Mn) and oxygen across the confined nanorods that crystallized in the form of MnO_2 nanoparticles and stabilizes the hexagonal MnO_2 phase prior to the LSMO phase formation.

The hexagonal unit cell determined in our MnO_2 nanowires has not been previously observed for any of the existing MnO_2 allotropes. Therefore, the MnO_2 nanowires formed at 700 °C with our growth method can be classified as a new nsutite ε-MnO_2 polytype with a new hexagonal unit cell.[33] The ε-MnO_2 class is based on a hexagonal packing of oxygen atoms with random occupancy of one-half the octahedral sites by manganese atoms.[34,35] The details of the structural arrangement of ε-MnO_2 are described as a random intergrowth of ramsdellite−pyrolusite chains, as proposed by De Wolff.[36] As a consequence of their

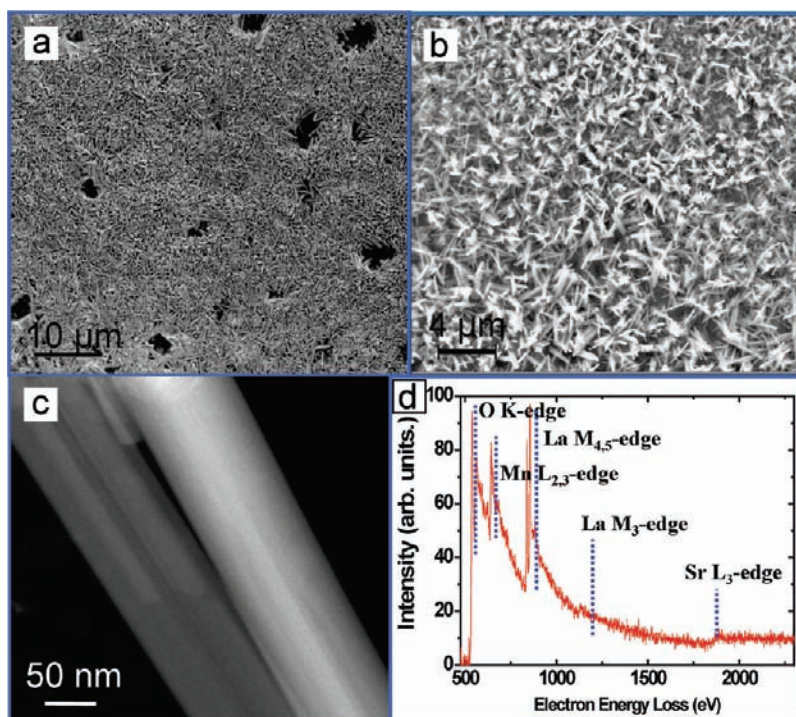**Figure 3.** (a) FE-SEM image of $La_{0.7}Sr_{0.3}MnO_3$ (LSMO) nanowires prepared using polycarbonate membranes with 100 nm pore size obtained after the high temperature thermal treatment at 1000 °C. (b) Magnified FE-SEM image of LSMO nanowires synthesized at 800 °C. (c) Scanning TEM image of two single LSMO nanowires. (d) High-resolution EELS analyses performed along a single LSMO nanowire.

highly anisotropic crystal lattice, the resulting crystals can spontaneously form regular morphologies under the appropriate reaction conditions. This fibrous morphology has been predominantly formed as nanowires,[12] well-aligned monocrystalline nanowires,[37] nanowire 3D nanostructures,[38] and nanorod 3D urchins.[14]

The design and fabrication of MnO_2 and their derivatives with 1D and 2D ordered structures have attracted the attention of chemists and materials scientists in the past few years.[10−18] When changing the chemical composition and the synthesis method of these oxides, very interesting and new structures with novel physical properties can be produced. A completely new situation arises by increasing the growth temperature in the range 800−1000 °C. Figure 3a shows the nanowires formed from a 1 μm thick PC template with 100 nm diameter pores filled with the precursor solution coating a (001)-silicon substrate after a high temperature treatment at 1000 °C for 5 h. As it can be seen in Figure 3b, the entire substrate area (1 cm^2) is covered with a high density of nanowires with diameters in the range 80−100 nm and lengths of up to 4 μm distributed randomly on the silicon substrate. Scanning transmission electron microscopy (STEM) images (Figure 3c) reveal that each nanowire has a uniform width along its entire length and smooth surface. EELS line scans on single nanowires determined that the nanowires are composed of La, Sr, Mn, and O and that the composition is uniform along the wires with no impurities present (see Figure 3d). In a previous work, we already confirmed that the electron diffraction patterns along different zone axes and the X-ray diffractograms can be indexed on the basis of a new monoclinic unit cell for LSMO with lattice parameters $a = 13.8$ Å, $b = 5.7$ Å, $c = 21.8$ Å, and $\beta = 101°$, and with the long axis of the nanowires along the b direction.[25] Figure 4a shows a high-resolution STEM image of a part of an individual nanowire obtained using a high angle annular dark

field (HAADF) detector, which is sensitive to the atomic number (Z-contrast)[39,40] along the [100] zone axis. In this projection, high contrast periodic fringes are observed. The distance between the parallel fringes is about 21.7 and 5.7 Å corresponding, respectively, to the spacing of the (001) and (010) planes of the LSMO monoclinic structure.[25] The power spectrum pattern generated by the Fourier transformation (see inset) shows that the LSMO nanowire is single crystalline and compatible with the determined monoclinic lattice. In a similar way, Figure 4b displays the HRSTEM image along the [001] zone axis, and the (100) and (010) interplanar distances are highlighted. Figure 4d presents a higher magnification STEM image of a LSMO nanowire along the [100] zone axis, and Figure 4e displays an atomic resolution EELS line scan along the arrow on Figure 4d. The image shows the rippling characteristics of atomic planes. The oxygen K, manganese $L_{2,3}$, and lanthanum $M_{4,5}$ edge positions are highlighted. Figure 4f shows a HAADF line scan along [001] (arrow on Figure 4d) and the simultaneously recorded EELS integrated intensities, extracted from the two-dimensional map in Figure 4e. The EELS line scans are consistent with the HAADF profile, because the HAADF contrast should be dominated by the Mn and La columns. The ripples in the O, La, and Mn signals along the scan line are a reflection of the positions of these elements. According to this element distribution, we propose a model structure for the LSMO nanowires grown at high temperatures, overlaid on Figure 4d, in which the La^{3+} (blue spheres) and Sr^{2+} (yellow spheres) cations are ordered inside the 1-D channels defined by the MnO_6 octahedra chains. This atomic distribution would explain the observed high-resolution EELS contrast and agrees also with the $La_{2/3}Sr_{1/3}MnO_{3+\delta}$ stoichiometry, because there are two La rows for each Sr row. Presumably, oxygen should be coordinated with these cations to stabilize the structure counteracting the repulsive
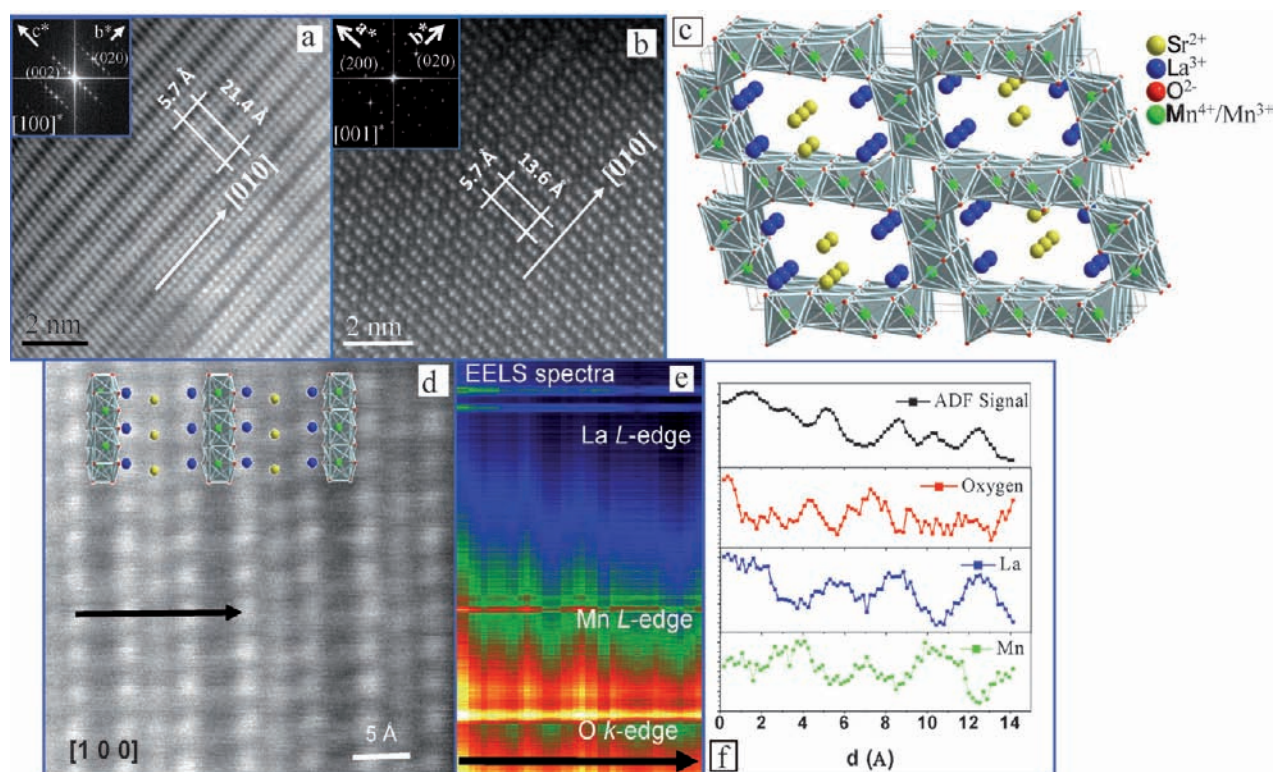
Figure 4. (a) Annular dark field (ADF) STEM image of a $La_{0.7}Sr_{0.3}MnO_3$ (LSMO) nanowire grown at 1000 °C along the [100] zone axis, obtained in a VG501 microscope. The inset shows the FFT of the image. (b) ADF image of a LSMO nanowire along the [001] zone axis. The inset shows the FFT of the image. (c) A drawing of the model LaSr-2 × 4 structure proposed for the LSMO nanowires. (d) Higher resolution image of a LSMO nanowire along the [100] zone axis. A LaSr-2 × 4 nanowire cell model has been highlighted on the ADF image, with yellow circles marking the Sr columns position, blue circles the La columns position, and red and green circles the O and Mn positions, respectively. (e) EELS line scan along the black arrow on (d), O−K, Mn−L$_{2,3}$, and La−M$_{4,5}$ edges positions are highlighted. The image shows the rippling characteristics of atomic resolution EELS. (f) From top to bottom: in black, ADF signal acquired simultaneously with the EELS line scan shown in (d); in red, O−K image obtained integrating the intensity under the O−K edge after background subtraction; in blue, La−M$_{4,5}$ image; and in green, Mn−L$_{2,3}$ image.

interaction between the positive charges of the La^{3+} and Sr^{2+} chains. Unfortunately, EELS could not resolve the oxygen positions. Very likely, to have this atomic arrangement, it is necessary to go to high enough temperatures (above 800 °C) to enhance atomic mobility. At lower growth temperatures, such as 700 °C, the La and Sr ions have not sufficient energy to overcome the diffusion barrier into the 1-D channels, and the formation of hexagonal ε-MnO$_2$ nanowires instead of LSMO nanowires is promoted.

A schematic model of the structure with a 2 × 4 tunnel arrangement is shown in Figure 4c. The isolated balls stand for the La^{3+} and Sr^{2+} cations, and the octahedra represent [MnO$_6$] units. The proposed structure is very similar to the RUB-7 type structure encountered in synthetic alkali manganates, which also have a one-dimensional (2 × 4) tunnel arrangement[31,32] except for the doubling of the lattice parameter along the channel axis b. The superstructure of the RUB-7 cell along the channel axis, with $b = 5.7$ Å ≈ $2b$(RUB-7), may arise from the particular arrangement of the La^{3+} and Sr^{2+} ions inside the tunnels. Our particular growth method has allowed the synthesis of manganate tunnel structures with simultaneous ordered arrangement of divalent and trivalent cations inside the channels for the first time. Because of the similarity with the previously synthesized Rb-2 × 4 and Na-2 × 4 structures, we designate our LSMO monoclinic nanowires as LaSr-2 × 4 tunnel structured nanowires.
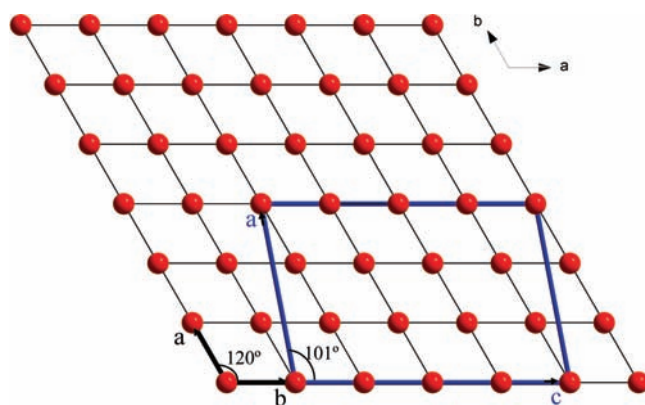

Figure 5. The relation between the *ab*-plane in the hexagonal ε-MnO$_2$ subcell and the *ac*-plane in the LaSr-2 × 4 monoclinic cell is displayed. The monoclinic supercell has 24 times larger unit cell volume.

Moreover, comparing the electron diffraction studies performed in the MnO$_2$ nanowires grown at 700 °C with the LSMO nanowires grown above 800 °C, we find that both crystallographic structures are closely related. In fact, as displayed in Figure 5, the LaSr-2 × 4 nanowires structure forms a crystallographic supercell corresponding to 24 times the volume of the hexagonal ε-MnO$_2$ unit cell. Our study of the distinct nanowires formation at mild (700 °C) and high (800−1000 °C)
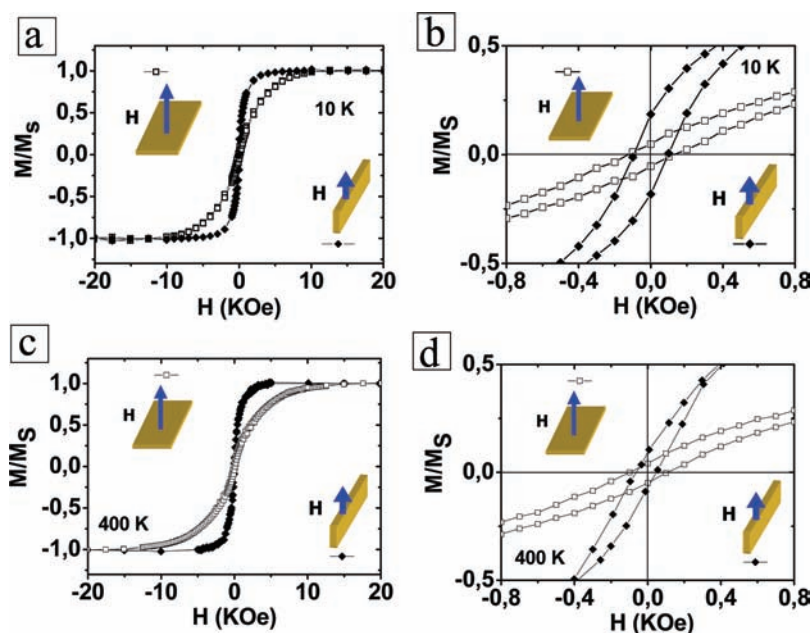
Figure 6. (a) Hysteresis loops of the LaSr-2 × 4 nanowires measured at 10 K for fields applied parallel (filled symbols), and perpendicular (open symbols), to the substrate plane. (b) Low field enlargement of the hysteresis loops measured at 10 K. (c) Hysteresis loops of the LaSr-2 × 4 nanowires measured at 400 K. (d) Low field enlargement of the hysteresis loops measured at 400 K.

temperatures results in the hypothesis that the formation of anisotropic monoclinic LSMO nanowires at temperatures above 800 °C is due to the fact that the crystallization of LSMO does not occur directly from the amorphous precursor, but through an intermediate MnO_2 crystalline phase that acts as a seed. This hexagonal and highly anisotropic intermediate phase influences the shape of the final LSMO crystallites. Hence, the MnO_2 nanocrystallites serve as the seeds for the growth of the LSMO nanowires through the diffusion of La and Sr in the empty 1D channels of hexagonal ε-MnO_2 promoted by the high temperature treatment. At low growth temperatures, the La and Sr ions have not sufficient energy to overcome the diffusion barrier into the channels, and the formation of LaSr-2 × 4 nanowires is hindered.

The confinement imposed by the nanoporous polymer template has a crucial influence on the inorganic phases formed. In particular, nucleation of crystalline ε-MnO_2 is not reached using porous templates with pores larger than 500 nm. In this case, vertical polycrystalline rhombohedral $R3$ LSMO nanorods are formed on top of the Si substrate (see Supporting Information Figure 4).

The interaction with the underlying substrate must also play an important role. When the nanoporous polymer templates cover the surface of (001)-$SrTiO_3$ or (001)-$LaAlO_3$, two substrates with perovskite structure and good lattice match to perovskite $La_{0.7}Sr_{0.3}MnO_3$, vertical polycrystalline perovskite $La_{0.7}Sr_{0.3}MnO_3$ nanorods are grown at mild temperatures (800 °C), and only upon strong thermal activation (1000 °C) do they suffer a profound transformation into vertical single crystalline $(La,Sr)_xO_y$ nanopyramids sitting on a $La_{0.7}Sr_{0.3}MnO_3$ epitaxial wetting layer.[27] In contrast, an amorphous SiO_2 layer is formed on the silicon substrate when submitted to the high temperature treatment in an oxidizing atmosphere (see inset in Figure 1a), and unanticipated effects occur as a consequence of the interplay among chemical compatibility, lattice mismatch, crystallographic structure, and interface and surface energies.

The very complex phenomenology displayed by the Mn— oxides as a function of their structural configuration makes highly appealing the investigation of the magnetic properties of the new monoclinic LSMO nanowires. For that purpose, magnetic hysteresis loops were measured at different temperatures between 10 and 500 K for fields up to 5T with the magnetic field applied in-plane and out-of-plane with respect to the substrate where the nanowires lie. The nanowires stand mainly parallel to the substrate, and they have a random azimuthal distribution of the long axis. Therefore, when the in-plane configuration is used, the magnetic field has a random distribution with the long axis of the nanowires, while in the out-of-plane configuration the magnetic field is always approximately perpendicular to the long axis of the nanowires. Figure 6a and c displays the magnetization curves measured at 10 and 400 K, while Figure 6b and d displays magnified images of the central part of the hysteresis loops. As observed, the in-plane magnetization curve leads to a saturated magnetization at a smaller magnetic field than does the out-of-plane curve, thus indicating that the direction perpendicular to the long axis of the nanowires is a hard axis magnetization direction. We have estimated a saturation magnetization value for the LSMO monoclinic nanowires phase at 10 K of 47 ± 10 emu/g, which is of the same order as the bulk perovskite $La_{0.7}Sr_{0.3}MnO_3$ saturation magnetization value (90 emu/g), indicating the high ferromagnetic strength of this new nanostructure. The large saturation magnetization value together with the strong magnetic anisotropy observed can not be explained if ferromagnetism had its origin in randomly distributed impurities or defects.

Figure 7 displays the temperature dependence of the magnetization, measured at an applied field of 1.5 T, for a polycrystalline perovskite LSMO sample and the monoclinic LaSr-2 × 4 nanowires, both prepared from the same chemical precursor solution. For the nanowires, the magnetization decreases at a slower rate with temperature, and still remains very high at 500 K (∼40% decrease from 5 K), thus indicating that the Curie
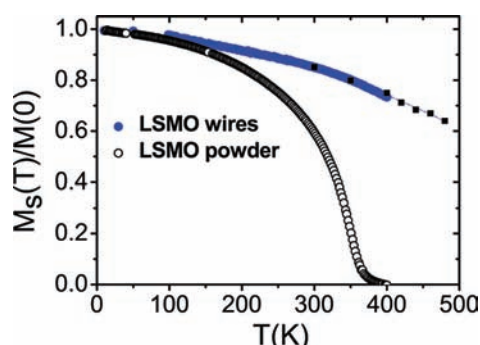
Figure 7. Temperature dependence of field-cooled magnetization at an applied magnetic field $H = 1.5$ T applied perpendicular to the substrate plane of the monoclinic LaSr-2 × 4 nanowires sample and of a perovskite powder reference sample. The discrete "■" points correspond to measurements performed with the vibrating sample magnetometer. The dotted line is a guide to the eyes.

temperature of the monoclinic LSMO nanowires is well above 500 K. This finding is very remarkable because T_c is much higher than all the well-established values reported so far for any perovskite Manganite compound. The origin of the observed high temperature ferromagnetism of these LaSr-2 × 4 nanowires must lie on the particular atomic arrangement of the manganese atoms in the monoclinic structure. The resulting interatomic distances may well modify the exchange interaction stabilizing a ferromagnetic configuration and, together with the coexistence of Mn^{3+} and Mn^{4+} cations, should be giving rise to the high temperature ferromagnetism observed.

Manganese compounds are known to have very interesting and complex magnetic behavior in addition to the rich phenomenology displayed by mixed-valent manganese oxide perovskites. Very often, there are competing interactions of opposite sign, caused by the direct and superexchange pathways.[41] This fact causes that apparently similar systems exhibit markedly different magnetic properties. In this way, in the lithium manganospinels,[42,43] for example, the ferromagnetic 90° $Mn^{4+}-O-Mn^{4+}$ interactions dominate against the antiferromagnetic $Mn^{4+}-Mn^{4+}$ interactions. This is in contrast with the magnetic behavior of the spinel λ-MnO_2 framework for which the antiferromagnetic $Mn^{4+}-Mn^{4+}$ interaction dominates due to a much smaller interatomic $Mn^{4+}-Mn^{4+}$ distance. Another example has been encountered in β-MnO_2, which shows a magnetic transition into a helical state at the Néel temperature $T_N \approx$ 92 K. However, coherently strained β-MnO_2 films heteroepitaxially grown on single crystal (001)-$LaAlO_3$ and (001)-MgO substrates display ferromagnetic behavior at room temperature, which was attributed to the change of the magnetic interaction by changing the interatomic distances.[44] Recently, ferromagnetic arrangement has been also measured in hexagonal ε-MnO_2 nanostructures with a Curie temperature of $T_c = 25$ K.[17,18] In our LaSr-2 × 4 nanowires, the chemical modification of ε-MnO_2 through its doping with La and Sr cations changes the crystallographic structure influencing the interatomic distances and induces mixed-valence Mn^{3+}/Mn^{4+}, the net effect being enhancement of the ferromagnetic interaction and the increase of T_c above room temperature.

■ CONCLUSIONS

In summary, we have presented a new synthesis route for MnO_2 and tunnel manganate nanowires based on solution chemistry combined with the use of nanoporous polymer templates supported on top of single crystalline silicon substrates. Because of the confined nucleation in high aspect ratio nanopores and of the high temperatures attained, new structures with novel physical properties can be produced by this bottom-up approach. At mild growth temperatures ($T_g = 700$ °C) up to 30 μm long, hexagonal ε-MnO_2 nanowires are generated, taking advantage of the large crystallographic anisotropy of ε-MnO_2. The nanocrystallites of MnO_2 formed at low temperatures serve as the seeds for the growth of LSMO nanowires through the diffusion of La and Sr into the empty 1D-channels of ε-MnO_2 at growth temperatures above 800 °C. Consequently, our particular growth method has allowed the synthesis of single crystalline (LaSr-2 × 4) molecular sieve monoclinic nanowires with ordered arrangement of the La^{3+} and Sr^{2+} cations inside the 1D-channels for the first time. These nanowires exhibit ferromagnetic ordering with strongly enhanced Curie temperature ($T_c > 500$ K) that probably results from the new crystallographic order between the La^{3+} and Sr^{2+} cations ordered inside the 2 × 4 1D-channels defined by the MnO_6 octahedra and from the mixed valence of manganese. The method developed in this work can be easily extended to other complex functional oxides to investigate new crystallographic phases and the modification of their physical properties.

■ ASSOCIATED CONTENT

Ⓢ **Supporting Information.** Figures displaying the reconstruction of the reciprocal lattice of the hexagonal ε-MnO_2 and the monoclinic $La_{0.7}Sr_{0.3}MnO_3$ (LSMO) nanowires, scanning TEM-EELS measurements of a single ε-MnO_2 nanowire grown at 700 °C, FE-SEM images of the ~1 μm diameter vertical polycrystalline LSMO nanorods, and profile matching refinement of the X-ray diffraction pattern of single crystalline LSMO monoclinic nanowires. This material is available free of charge via the Internet at http://pubs.acs.org.

■ AUTHOR INFORMATION

Corresponding Author
narcis.mestres@icmab.es

■ REFERENCES

(1) Chappert, C.; Fert, A.; Van Dau, F. N. *Nat. Mater.* **2007**, 6, 813–823.

4060

dx.doi.org/10.1021/ja1098963 |*J. Am. Chem. Soc.* 2011, 133, 4053–4061

(2) Beaulac, R.; Schneider, L.; Archer, P. I.; Bacher, G.; Gamelin, D. R. *Science* **2009**, *325*, 973–976.

(3) May, S. J.; Ryan, P. J.; Robertson, J. L.; Kim, J.-W.; Santos, T. S.; Karapetrova, E.; Zarestky, J. L.; Zhai, X.; te Velthuis, S. G. E.; Eckstein, J. N.; Bader, S. D.; Bhattacharya, A. *Nat. Mater.* **2009**, *8*, 892–897.

(4) Tokura, Y. *Rep. Prog. Phys.* **2006**, *69*, 797–851.

(5) Hwang, H. Y.; Cheong, S. W. *Nature* **1997**, *389*, 942–944.

(6) Coey, J. M. D.; Venkatesan, M.; Fitzgerald, C. B. *Nat. Mater.* **2005**, *4*, 173–179.

(7) Radaelli, P. G. *New J. Phys.* **2005**, *7*, 53–76.

(8) Özgür, Ü. A.; Morkoç, H. *J. Mater. Sci.: Mater. Electron.* **2009**, *20*, 789–834.

(9) D Serrate, e. a. *J. Phys.: Condens. Matter* **2007**, *19*, 023201–023287.

(10) Suib, S. L. *Acc. Chem. Res.* **2008**, *41*, 479–487.

(11) Suib, S. L. *J. Mater. Chem.* **2008**, *18*, 1623–1631.

(12) Cheng, F.; Chen, J.; Gou, X.; Shen, P. *Adv. Mater.* **2005**, *17*, 2753–2756.

(13) Ghodbane, O.; Pascal, J.; Favier, F. *ACS Appl. Mater. Interfaces* **2009**, *1*, 1130–1139.

(14) Li, W. N.; Yuan, J.; Shen, X.; Gomez-Mower, S.; Xu, L.-P.; Sithambaram, S.; Aindow, M.; Suib, S. *Adv. Funct. Mater.* **2006**, *16*, 1247–1253.

(15) Espinal, A. E.; Zhang, L.; Chen, C.; Morey, A.; Nie, Y.; Espinal, L.; Wells, B. O.; Joesten, R.; Aindow, M.; Suib, S. L. *Nat. Mater.* **2010**, *9*, 54–59.

(16) Ge, J.; Zhuo, L.; Yang, F.; Tang, B.; Wu, L.; Tung, C. *J. Phys. Chem. B* **2006**, *110*, 17854–17859.

(17) Ding, Y. S.; Shen, X. F.; Gomez, S.; Luo, H.; Aindow, M.; Suib, S. *Adv. Funct. Mater.* **2006**, *16*, 549–555.

(18) Liu, Y.; Wang, H.; Zhu, Y.; Wang, X.; Liu, X.; Li, H.; Qian, Y. *Solid State Commun.* **2009**, *149*, 1514–1518.

(19) Zhu, D.; Zhu, H.; Zhang, Y. *Appl. Phys. Lett.* **2002**, *80*, 1634–1636.

(20) Zhang, T.; Jin, C. G.; Qian, T.; Lu, X. L.; Bai, J. M.; Li, X. G. *J. Mater. Chem.* **2004**, *14*, 2787–2789.

(21) Schwartz, R. W.; Schneller, T.; Waser, R. *C. R. Chim.* **2004**, *7*, 433–461.

(22) Bhuiyan, M. S.; Paranthaman, M.; Salama, K. *Supercond. Sci. Technol.* **2006**, *19*, R1–R21.

(23) Gutierrez, J.; Llordes, A.; Gazquez, J.; Gibert, M.; Roma, N.; Ricart, S.; Pomar, A.; Sandiumenge, F.; Mestres, N.; Puig, T.; Obradors, X. *Nat. Mater.* **2007**, *6*, 367–373.

(24) Gibert, M.; Puig, T.; Obradors, X.; Benedetti, A.; Sandiumenge, F.; Hühne, R. *Adv. Mater.* **2007**, *19*, 3937–3942.

(25) Carretero-Genevrier, A.; Mestres, N.; Puig, T.; Hassini, A.; Oro, J.; Pomar, A.; Sandiumenge, F.; Obradors, X.; Ferain, E. *Adv. Mater.* **2008**, *20*, 3672–3677.

(26) Moreno, C.; Abellán, P.; Hassini, A.; Ruyter, A.; Pino, A. P. d.; Sandiumenge, F.; Casanove, M.; Santiso, J.; Puig, T.; Obradors, X. *Adv. Funct. Mater.* **2009**, *19*, 3672–3677.

(27) Carretero-Genevrier, A.; Gázquez, J.; Puig, T.; Mestres, N.; Sandiumenge, F.; Obradors, X.; Ferain, E. *Adv. Funct. Mater.* **2010**, *20*, 2139–2146.

(28) Hernandez, B. A.; Chang, K.; Fisher, E. R.; Dorhout, P. K. *Chem. Mater.* **2002**, *14*, 480–482.

(29) Leyva, A. G.; Stoliar, P.; Rosenbusch, M.; Lorenzo, V.; Levy, P.; Albonetti, C.; Cavallini, M.; Biscarini, F.; Troiani, H. E.; Curiale, J.; Sanchez, R. D. *J. Solid State Chem.* **2004**, *177*, 3949–3953.

(30) Shankar, K. S.; Raychaudhuri, A. K. *Nanotechnology* **2004**, *15*, 1312–1316.

(31) Rziha, T.; Gies, H.; Rius, J. *Eur. J. Mineral.* **1996**, *8*, 675–686.

(32) Xia, G.; Tong, W.; Tolentino, E. N.; Duan, N.; Brock, S. L.; Wang, J.; Suib, S. L.; Ressler, T. *Chem. Mater.* **2001**, *13*, 1585–1592.

(33) Zwicker, W. K.; Meijer, W. O.; Jaffe, H. W. *Am. Mineral.* **1962**, *47*, 246.

(34) Brenet, J. *J. Power Sources* **1992**, *39*, 349–368.

(35) De Wolff, P. M.; Visser, J. W.; Giovanoli, R.; Bruetsch, R. *Chimia* **1978**, *32*, 257–259.

(36) De Wolff, P. M. *Acta Crystallogr.* **1959**, *12*, 341–345.

(37) Xiong, Y.; Xie, Y.; Li, Z.; Wu, C. *Chem.-Eur. J.* **2003**, *9*, 1645–1651.

(38) Wu, C.; Xie, Y.; Wang, D.; Yang, J.; Li, T. *J. Phys. Chem. B* **2003**, *107*, 13583–13587.

(39) Pennycook, S. J.; Jesson, D. E. *Acta Metall. Mater.* **1992**, *40*, S149–S159.

(40) Batson, P. E.; Dellby, N.; Krivanek, O. L. *Nature* **2002**, *418*, 617–620.

(41) Masquelier, C.; Tabuchi, M.; Ado, K.; Kanno, R.; Kobayashi, Y.; Maki, Y.; Nakamura, O.; Goodenough, J. B. *J. Solid State Chem.* **1996**, *123*, 255–266.

(42) Branford, W.; Green, M. A.; Neumann, D. A. *Chem. Mater.* **2002**, *14*, 1649–1656.

(43) Mukai, K.; Sugiyama, J. *Solid State Commun.* **2010**, *150*, 906–909.

(44) Xing, X. J.; Yu, Y. P.; Xu, L. M.; Wu, S. X.; Li, S. W. *J. Phys. Chem. C* **2008**, *112*, 15526–15531.